

# Climate signals from SSM/I observations of marginal ice shelves

J. K. RIDLEY

*University College London, Mullard Space Science Laboratory, Holmbury St. Mary, Dorking, Surrey RH5 6NT, U.K.*

**ABSTRACT.** A time series of satellite passive microwave observations by the Special Sensor Microwave/Imager (SSM/I) instrument, of the Antarctic marginal ice shelves, reveals sharp transitions in the radiometric brightness temperatures at 19 and 37 GHz. These transitions, sometimes occurring over the period of a single day, indicate the onset of surface melting of the ice. Monitoring the day of the onset of melting and the permanent re-freezing will be a measure of rising air temperatures as a result of global warming. The response from a stable ice shelf, the Ronne, where no appreciable melting occurs, is compared with observations from the marginal ice shelves on Antarctic Peninsula. It is observed that the spectral gradient ( $T_{b19} - T_{b37}$ ) varies as a function of time on a clear annual cycle. It is shown that variations in the spectral gradient arise due both to the temperature profile within the snow and the dielectric effects of a wet surface layer.

## INTRODUCTION

It has been observed that several ice shelves off the coast of the Antarctic Peninsula exist close to the climatic limit of variability, taken by Mercier (1978) to be the 0°C summer isotherm. Morrison (1990) presented mean annual air temperature records for Faraday station (since 1957) that show an increase of 1.5°C to date. For a further discussion of this subject see Vaughan and others (1993). It is expected that rising air temperatures will lead to an increase in melting on the surface of ice shelves and we wish to investigate if this is detectable using space-borne microwave instruments.

Microwave observations, both passive and active, of snow are sensitive to surface moisture variations and so provide useful climatic and glaciological information concerning the continent-wide annual variation of surface physical state and temperature. However, physical models are required of the surface characteristics to enable a greater understanding of the satellite measurements. Three full years, from July 1987 to June 1990, of SSM/I data from daily mean grids of Antarctica are used. Brightness temperatures are expressed as  $T_{bv}$ , at frequencies of 19 and 37 GHz. Discussed here are observations of variations, both geographically and annually, in the times of onset of melting and refreezing over the austral summer, and how these will serve as direct indicators of rising air temperatures over large areas. Continual monitoring of the freeze-thaw cycle of the surface snow, on an annual basis, will serve as a climatic indicator.

## THE DATA SET

The Defense Meteorological Satellite Program F-8

platform was launched into a sun-synchronous orbit on 20 June 1987 and continues to operate to date. One of the instruments on board is the Special Sensor Microwave/Image (SSM/I), a seven-channel, four-frequency, linearly polarised, passive microwave radiometric system. The instrument measures atmospheric/surface brightness temperatures at 19.3, 22.2, 37.0 and 85.5 GHz. The sensor samples every 12.5 km along track at 85.5 GHz, every 25 km along track at lower frequencies. Coverage is global except poleward of 87° N and 87° S.

The swath data have been processed by the National Snow and Ice Data Centre and gridded at 12.5 km resolution for 85.5 GHz and 25 km for the lower frequencies, on north and south polar stereographic grids. The grid values are the mean brightness temperature over a 24-hour period. A major data gap is present during the period from 3 December 1987 to 12 January 1988, when the sensor was turned off due to instrument overheating caused by solar radiation.

In this study the SSM/I South Polar Region dataset was used providing gridded daily observations on CD-ROM from 9 July 1987 to 30 June 1990. Only the data from the 19 GHz and 37 GHz channels were used as these brightness temperatures are least affected by atmospheric conditions. Single pixel data, over three years, for  $T_{b19}$  and  $T_{b37}$ , from selected locations on the south polar grid, correspond to points on the principle ice shelves bordering Antarctic Peninsula (Fig. 1).

## OBSERVATIONS

In a fashion similar to passive microwave observations of diurnal permafrost melting (England, 1990), it is observed that the spectral gradient,  $\Delta T_b =$

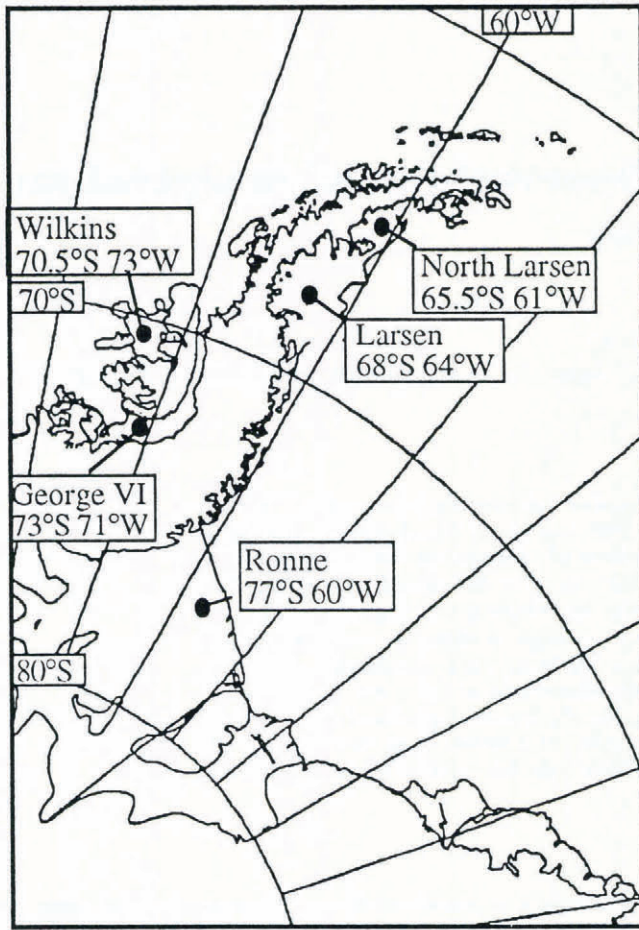


Fig. 1. Location diagram of sites around Antarctic Peninsula for which annual brightness temperature variations were investigated.

( $T_{b19} - T_{b37}$ ), of snow on the selected ice shelves varies as a function of time on an annual cycle. The spectral gradient over permanently dry snow is principally due to scattering of the snow grains (Chang and others, 1976; Zwally and Gloersen, 1977). Variations in the spectral gradient, assuming no change in grain size, will be due to changes in the physical temperature profile. Snow at the effective depth of the 19 GHz radiation is at a different physical temperature from that of the lesser effective depth at 37 GHz. During the austral winter the surface snow is cooler than that at depth and the spectral gradient is positive whilst in the austral summer the physical temperature gradient is reversed and the spectral gradient becomes negative.

The time series of the 19 GHz channel over three years, of the data over the George IV Ice Shelf, which is typical for all the ice shelves observed except the Ronne, is shown in Figure 2a. Temperature increases linearly throughout the year until the first melting occurs, indicated by a spike in the brightness temperature. The spike is normally followed by a fall back to the preceding temperature ramp, indicating re-freezing, but a subsequent block of high brightness temperatures are due to the higher emissivity of wet snow over dry snow. Summer is usually followed by a further number of short freeze-thaw cycles. The corresponding spectral gradient (Fig. 2b) shows a sharp rise for each melt incidence, followed by a slow exponential decay as the frozen layers are buried by accumulation or degraded by wind ablation. The start and end of the melt season are determined by a half-peak threshold in the brightness

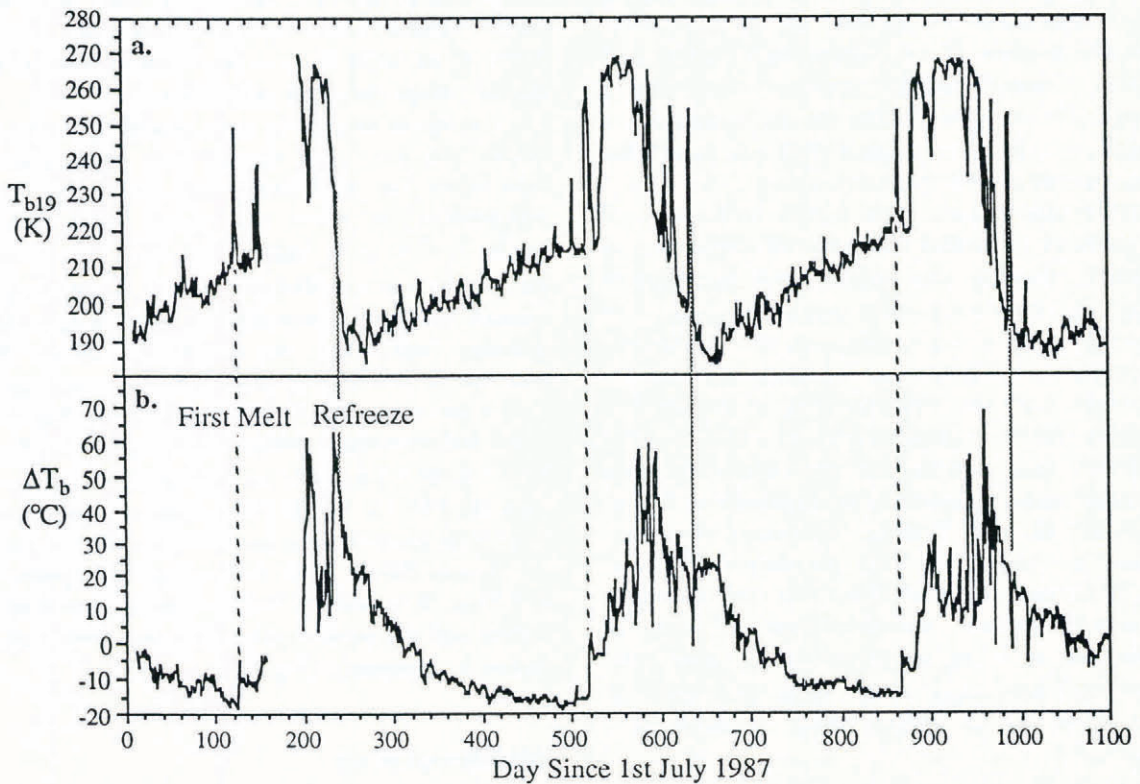


Fig. 2. The three-year times series of observations of radio brightness for George VI Ice Shelf. (a) 19 GHz (vertical polarization) brightness temperature, (b) difference between the 19 GHz and 37 GHz (vertical polarization) brightness temperatures, showing the points of annual surface melt and refreeze.

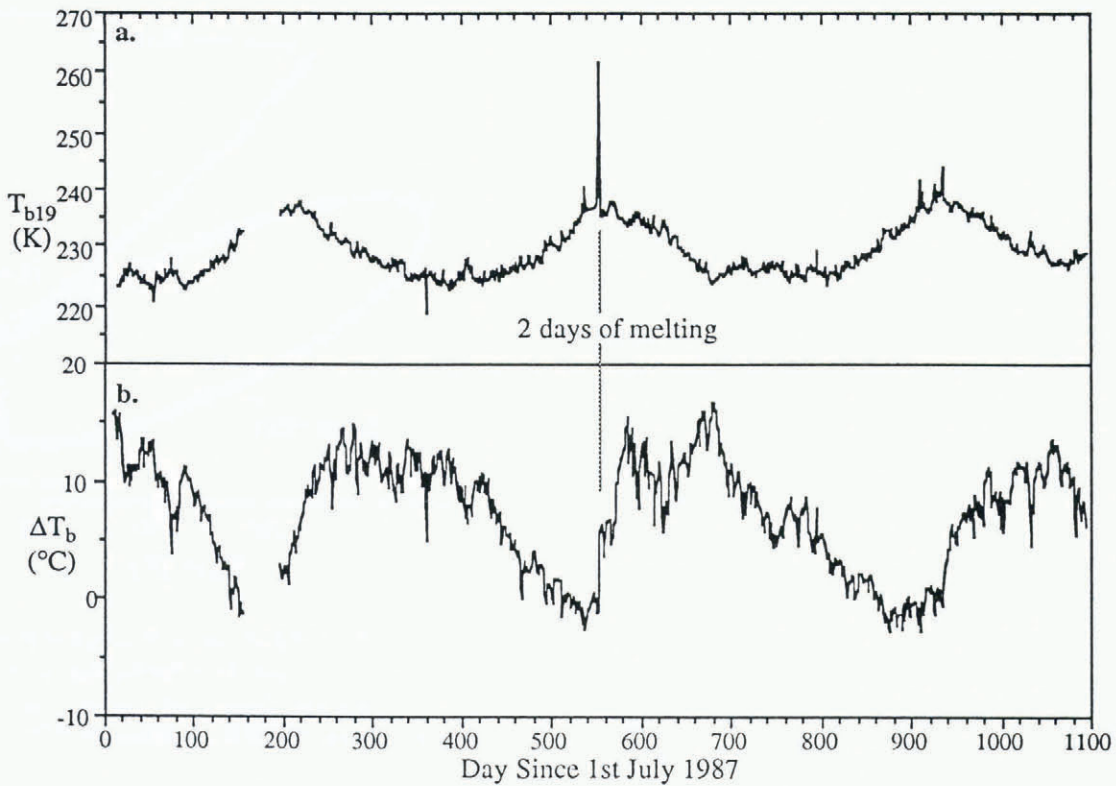


Fig. 3. The three-year time series of observations of radio brightness for Ronne Ice Shelf. (a) 19 GHz (vertical polarization) brightness temperature, (b) difference between the 19 GHz and 37 GHz (vertical polarization) brightness temperatures, showing the single time in January 1989 when surface melting briefly seemed to occur.

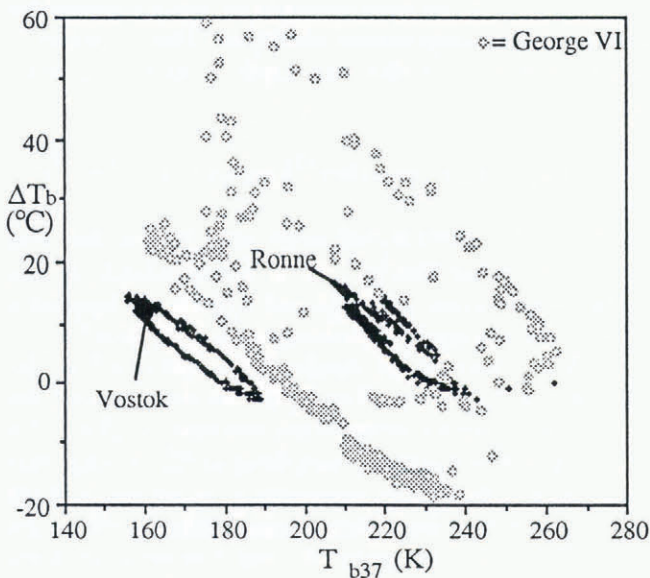


Fig. 4. A scatterplot of  $T_{b19} - T_{b37}$  showing the close oval distributions for areas with no surface melting (Vostok and Ronne Ice Shelf) and the quite dispersed distribution where there is melting on the George VI Ice Shelf.

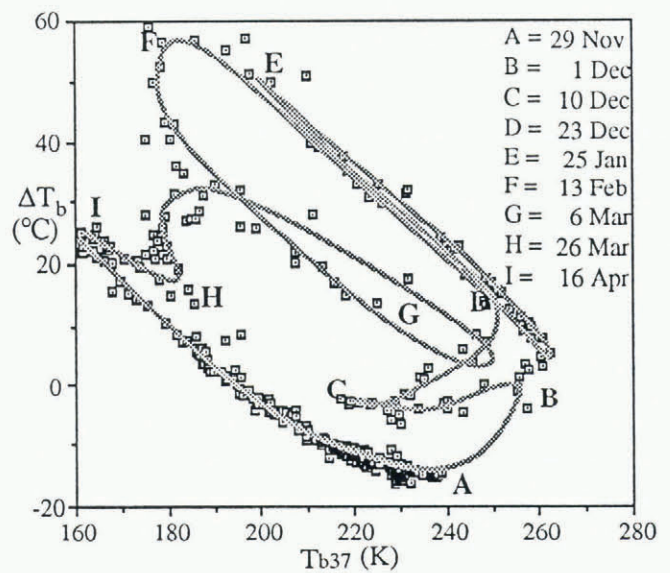


Fig. 5. Detail of the time track followed by a point on the George VI Ice Shelf on the scatterplot of  $T_{b19} - T_{b37}$  against  $T_{b37}$  over the course of a year (July 1988–June 1989).

temperature (230 K in Fig. 2a), and the start is confirmed through the associated sharp rise in  $\Delta T_b$ .

The contrast to the radio-brightness time profiles for the George VI Ice Shelf, with those for the Ronne Ice Shelf (Fig. 3), shows what occurs on an ice shelf with no significant surface melting. The annual brightness

temperature range at 19 GHz is only 15°C (30°C for 37 GHz) and  $\Delta T_b$  is around 15°C, compared with 70°C on George VI. The time series of  $\Delta T_b$  (Fig. 3b) show no high gradients as seen in Figure 2b, except on 4 January when a freak warm day seems to have occurred, resulting in a partial melting of the surface snow.

Plots of the spectral gradient against  $T_{b37}$  over snowpack reveal that the brightness temperature follows a distinct path through the range of spectral gradients. For locations on the Antarctic plateau, and for southerly ice shelves, such as the Ronne and the Ross, this path is a simple hysteresis track as shown for Vostok (78°28' S, 106°49' E) and Ronne in Figure 4. This effect is a function of the velocity of propagation of the annual temperature minimum, which is in turn a function of the thermal diffusivity of the firn and the frequency of the surface temperature change. The two microwave frequencies are observing at different effective depths in the snow, 37 GHz at about 0.2 m and 19 GHz at about 1 m. However, when the radio-brightness of marginal ice shelves bordering the Antarctic Peninsula is investigated, a new regime in the scatterplot is revealed, together with two distinct physical properties for the observed surface, corresponding to summer and winter. George VI Ice Shelf is typical in this respect (Fig. 5).

The physical change is demonstrated to be due to surface melting through modelling of the dielectric properties of the snow when dry and wet. The transition between these two states is always very rapid (one or two days) during melt in spring, but is characterised during autumn by a series of freeze-thaw cycles. The times of onset of melt and re-freezing are correlated with latitude but are variable from year to year although the shape of the scatterplot remains essentially the same with time and location. The water content of the snow may be determined through modelling of the emission processes (Ulaby and others, 1986). Variations in these factors are possible indicators of climatic change.

**MICROWAVE PROPERTIES OF SNOW**

At a particular frequency,  $\nu$ , the brightness temperature,  $T_b$ , is a function of the true temperature,  $T$ , given by

$$T_{b\nu} = e(1 - a)T,$$

where  $e$ , the surface emissivity, is a function of the frequency and the surface dielectric constant. The scattering albedo,  $a$ , of the medium is one of the key parameters determining the behaviour of snow emission. It is governed by the ice-particle size relative to the observed radiation wavelength as described by the bulk scattering,  $\kappa_s$ , and absorption,  $\kappa_a$ , coefficients:

$$a = \kappa_s / (\kappa_s + \kappa_a).$$

At a given frequency, the input parameters necessary to specify  $\kappa_s$  and  $\kappa_a$  for dry snow are the snow density, the radius of the ice particle and the physical temperature of the snow medium. For wet snow we additionally need to specify the liquid-water content,  $m_v$ . At frequencies above 20 GHz, scattering becomes the dominant component of the total extinction loss of the medium. Thus the magnitude of  $T_{b37}$  compared to  $T_{b19}$  is an indication of the scattering strength of the medium.

When snow melts, the absorption coefficient increases from practically zero for dry snow to a larger value than  $\kappa_s$  for  $m_v > 1\%$ . Thus, the presence of a very small amount of liquid water in a snow mixture is sufficient to reduce the magnitude of the scattering albedo to a very

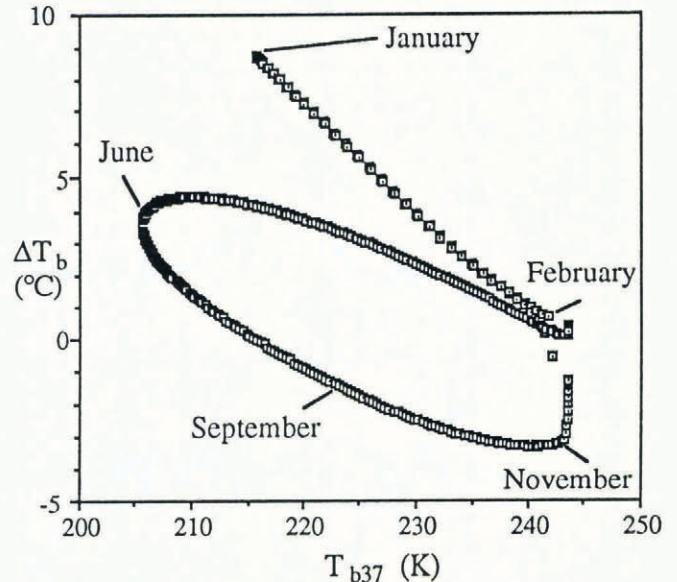


Fig. 6. The time track followed, in 37 GHz and brightness temperature gradient space, by a theoretical point on an ice shelf whose surface follows an annual sinusoid in temperature (mean = 255 K, amplitude = 25°C).

small value and the apparent temperature dependence on the grain radius is much reduced.

The simple radiative transfer model, based on that of England (1990), has been constructed, using a sinusoidal annual surface-temperature variation. This produces a snow-temperature profile with depth,  $z$ , at time  $t$ , given by:

$$T(z, t) = T_s \exp\{-z(\omega/2k)^{1/2}\} \sin\{\omega t - z(\omega/2k)^{1/2}\}$$

where  $k$  is the thermal diffusivity given by Carslaw and Jaeger (1959) as  $36\text{m}^2\text{a}^{-1}$ ,  $T_s$  is the amplitude of the surface-temperature variation and  $\omega/2\pi$  is the frequency of the surface-temperature change (once per year).

A linear increase in density from  $300\text{kg m}^3$  at the surface to  $500\text{kg m}^3$  at 10 m depth was assumed and the amplitude of surface temperature variation of  $25^\circ\text{C}$ . The mean annual temperature was fixed at 255 K such that peak summer surface air temperature would reach 280 K with an estimated snow-water content rising to 3% in the surface layers. The emission and transmission from discrete layers to the surface was calculated and summed for all layers. After correcting for scattering attenuation from snow grains 0.2 mm in diameter, and surface transmission at the  $50^\circ$  incidence angle of SMM/I, we can approximate the radiative properties through  $\Delta T_b$  and  $T_b$  space as shown in Figure 6.

**DISCUSSION**

The time track of the radiative properties through  $\Delta T_b$  and  $T_b$  space always follows a simple oval path when there is no surface melting. Melting, which results in 1–2% by volume of liquid water content in the snow, always produces a second, linear, track on the plot which can be

clearly identified. The brightness temperature moves up and down this line as the water content of the snow surface changes with atmospheric conditions.

The numerical model of an arbitrary snow medium, described above, reproduces the general shape of the time tracks when a sinusoidal annual surface temperature variation is assumed. However, it is clear from Figure 2a that the snow temperature does not follow a sine wave, rather it seems to follow a saw-tooth pattern with a rapid drop off in temperature following the end of the summer melting. This being the case, the February–June stretch of the model track in Figure 6 should be much sparser in data points (one point per day) as is the case in region G of Figure 4. The model does not predict the excursions in Figure 4 during melt (region C) and freeze-up (region F). The former would require a more detailed model for how the water content varies with increasing air temperature, and there is also an effect due to the latent heat of fusion to be taken into account in future studies. The scatter of points in region F, where  $\Delta T_b$  is high, seems to be due to the formation of a hard crust with a number of days of surface melt followed by re-freezing at night. The emissivity of re-frozen snow has a strong negative gradient with microwave frequency as the ice grains are much larger than winter grains, and hence scattering loss is increased at higher frequencies (Schanda and others, 1983) and  $\Delta T_b$  is high. This is supported by the incidental observation that the degree of polarization of the radiation at both 19 and 37 GHz drops significantly at the end of the summer, again indicating that incoherent volume scattering is the dominant effect.

All the marginal ice shelves display plots similar to those shown in Figures 2 and 4, with variations only in the time scheduling of the features and minor differences in the mean annual brightness temperatures. In all cases, with the onset of melting, a discontinuity appears on the time profile of  $\Delta T_b$  as shown in Figure 2b. This corresponds to the gap in the track in Figure 4 between points A and B. The identification of the point of re-freezing is complicated by the presence of crusts, the diurnal thaw and re-freezing cycle and the rate at which new accumulation buries or ablates these crusts. The times for the onset and approximate end of melting for three years of the data are presented in Table 1.

The Ronne Ice Shelf does not exhibit the signature of

surface melting of the more northerly ice shelves, however on 4 January 1989 it did show a deviation from the normal hysteresis pattern. Such a deviation indicates a small transient presence of liquid water. If these “freak” periods of melting on the Ronne become more frequent, then this would be a further indication of rising air temperatures and changing weather patterns. Like the marginal ice shelves, the Ronne shows moderate deviations in  $\Delta T_b$  during winter and these are probably due to variations in the snow-grain size from old snow to fresh snow following snowfall.

The Peninsula ice shelves can be geographically split between the east (Larsen) and west (Wilkins and George VI) sides of the Peninsula. The main Larsen Ice Shelf seems to have a very regular melt cycle and this is the shortest period of melt of the four. The northern Larsen is more erratic in its pattern, possibly reflecting greater climatic variability with lower latitude. Like the two western ice shelves, it experienced an exceptionally early melt in 1987. Whilst missing data inhibit a detection of the melt that year for the central Larsen, it is clear that this was later than 2 December and hence unrelated to that of the other shelves. The western ice shelves have melt cycles which are closely linked with melt and freeze dates which are practically identical and longer periods of melt than the northern Larsen. The spread of 28 days in the thaw dates across three years indicates considerable regional climatic variability.

## CONCLUSIONS

Surface melting on snow is detectable using satellite passive microwave instruments, the time of onset of melting is rapid and can be determined to the time resolution of the SSM/I gridded data of one day. Surface melting is detected on all the major Antarctic Peninsula ice shelves but not on the Ronne Ice Shelf. As air temperatures rise the Ronne may incur some melting and the spread of melt area on a year-by-year basis may be mapped. With only three years of data it is not possible to state if the variability in the start and length of time of melting on the ice shelves is typical, but the central Larsen Ice Shelf appears quite stable in these respects.

The passive microwave data display additional features of the melt and re-freeze process which may reveal information about the local accumulation rates as snow builds up over re-frozen crusts.

## ACKNOWLEDGEMENTS

The author acknowledges financial support from NERC-BAS Special Topic grant and the free provision of the SSM/I data from NSIDC. Thanks are also given to S. Laxon and S. Brown of MSSL for software support.

## REFERENCES

- Carslaw, H. S. and J. C. Jaeger. 1959. *Conduction of heat in solids. Second edition.* Oxford, Clarendon Press.  
Chang, T. C., P. Gloersen, T. Schmugge, T. T. Wilheit

Table 1. The dates (day/month) of annual thaw and final freezing of the ice shelves under observation 1987–90

Location	Thaw : freeze 1987–88	Thaw : freeze 1988–89	Thaw : freeze 1989–90
Larsen	? : 22/2	4/12 : 31/1	4/12 : 12/2
Larsen-North	2/11 : 18/2	2/12 : 3/3	5/12 : 16/3
George VI	2/11 : 22/2	30/11 : 8/3	13/11 : 16/3
Wilkins	2/11 : 23/2	29/11 : 9/3	13/11 : 16/3
Ronne	None	None	None

- and H.J. Zwally. 1976. Microwave emission from snow and glacier ice. *J. Glaciol.*, **16**(74), 23–39.
- England, A.W. 1990. Radiobrightness of diurnally heated, freezing soil. *IEEE Trans. Geosci. Remote Sensing*, **GE-28**(4), 464–476.
- Mercer, J.H. 1978. West Antarctic ice sheet and CO<sub>2</sub> greenhouse effect: a threat of disaster. *Nature*, **271**(5643), 321–325.
- Morrison, S.J. 1990. Warmest year on record on the Antarctic Peninsula? *Weather*, **45**(6), 231–232.
- Schanda, E., C. Mätzler and K. Künzi. 1983. Microwave remote sensing of snow cover. *Int. J. Remote Sensing*, **4**(1), 149–158.
- Ulaby, F.T., R.K. Moore and A.K. Fung. 1986. *Microwave remote sensing: active and passive. Volume III.* Norwood, MA., Artech House.
- Vaughan, D.G., D.R. Mantripp, J. Sievers and C.S.M. Doake. 1993. A synthesis of remote sensing data on Wilkins Ice Shelf, Antarctica. *Ann. Glaciol.*, **17** (see paper in this volume).
- Zwally, H.J. and P. Gloersen. 1977. Passive microwave images of the polar regions and research applications. *Polar Rec.*, **18**(116), 431–450.

*The accuracy of references in the text and in this list is the responsibility of the author, to whom queries should be addressed.*